Simple Precision Creation of Digitally Specified, Spatially Heterogeneous, Engineered Tissue Architectures

Umut Atakan Gurkan, Yantao Fan, Feng Xu, Burcu Erkmen, Emel Sokullu Urkac, Gunes Parlakgul, Jacob Bernstein, Wangli Xing, Edward S. Boyden,* and Utkan Demirci**

Natural organs are spatially heterogeneous, both in material composition and in the cell types within. Engineered tissues, in contrast, remain challenging to create, especially if the goal is to spatially position multiple cell types in a heterogeneous pattern in three dimensions (3D). Here, we describe a simple, inexpensive, yet extremely precise method to create tissue architectures in a digitally specifiable fashion, with morphological and compositional tuning. Specifically, we pattern hydrogel crosslinking via a novel photolithographic process that can trap solutions of extracellular matrix (ECM) components, cells, and diffusible factors in defined 3D shapes, without requiring specialized expensive optics or robotics. By iterating this process with different patterns and different cellular compositions, engineered tissues of varying heterogeneity, size, and complexity can be designed and implemented with microscale precision, in a fashion practical for individual laboratories to perform. We demonstrate the power of this process by engineering tissue building blocks in defined geometries, creating engineered tissues that encapsulate different cells (e.g., primary neurons, embryonic stem cells (ESCs), human umbilical vein endothelial cells (HUVECs), and fibroblasts) at specified locations throughout a single 3D tissue volume. We used the ability to rapidly synthesize tissue volumes of varying scale to examine how tissue volume governs neuron development.

Native tissues consist of multiple cell types and ECM components, which are spatially heterogeneous and organized in a three-dimensional (3D) environment.[1–6] Precision spatial positioning of cells and ECM components is crucial for natural tissue development and function.[3,5,7–12,13] Engineered tissues have been difficult to generate with comparable degrees of material and cell type spatial variability found in natural tissues. Current technologies can pattern cells on a two-dimensional (2D) substrate, providing control over composition and spatial arrangement on a flat surface.[14] However, cells anchored on 2D substrates do not recapitulate important features of cell behavior in vivo, such as cell-cell and cell-microenvironment interactions in 3D.[4–5,9–10,15,16] A current challenge is to develop 3D tissue constructs that replicate the architecture and cellular complexity found in vivo[2,10,15,17] for more accurate platforms for basic science, drug screening and diagnostic platforms, and also for prototyping tissues for clinical replacement. For example, for the brain, which has perhaps thousands of different kinds of cells, arranged in complex 3D architecture, fundamentally new kind of tissue engineering techniques might be required.[18–22]

In recent years, many strategies have been proposed for how to define the cellular architectures of engineered tissues in 3D,[5,23–33] but an overall technological pipeline capable of simple, inexpensive, practical, and powerful generation of spatially varying, micron-scale precise, and complex physiological systems, is needed. For example, existing strategies that could be used for the creation of 3D spatially complex engineered tissues (e.g., stereolithography, bioprinting, assembly, and casting) either do not provide degrees of freedom in all three dimensions, essential for defining 3D spatially varying cellular organization, or the cost and time budget rise exponentially as the resolution is pushed to cellular scales (i.e., 10–20 μm), and as the structure dimensions are pushed to centimeter scales–critical for creating 3D spatially varying model tissues of importance for biology and medicine.

Dr. U. A. Gurkan,[+] Y. Fan,[+] Dr. F. Xu, B. Erkmen, Dr. E. S. Urkac, G. Parlakgul
Harvard Medical School
Division of Biomedical Engineering at Brigham and Women's Hospital
Bio-Acoustic-MEMS in Medicine (BAMM) Laboratory
Harvard-MIT Health Sciences & Technology
65 Landsdowne St. PRB 252, Cambridge, MA 02139, USA

J. Bernstein
Media Lab and McGovern Institute
Departments of Brain and Cognitive Sciences and Biological Engineering
Massachusetts Institute of Technology
Cambridge, Massachusetts 02139, USA

Dr. W. Xing
Medical Systems Biology Research Center
School of Medicine
Tsinghua University
Beijing 100084, PR China
National Engineering Research Center for Beijing Biochip Technology
18 Life Science Parkway, Beijing, 102206, P. R. China
E-mail: wlxing@tsinghua.edu.cn

Dr. E. S. Boyden
Media Lab and McGovern Institute
Departments of Brain and Cognitive Sciences and Biological Engineering
Massachusetts Institute of Technology
Cambridge, Massachusetts 02139, USA
E-mail: edboyden@mit.edu

Dr. U. Demirci
Harvard Medical School
Brigham and Women's Hospital
Harvard-MIT Health Sciences & Technology
65 Landsdowne St. PRB 252, Cambridge, MA 02139, USA
E-mail: udemirci@rics.bwh.harvard.edu

[+] These authors contributed equally to this work.

DOI: 10.1002/adma.201203261

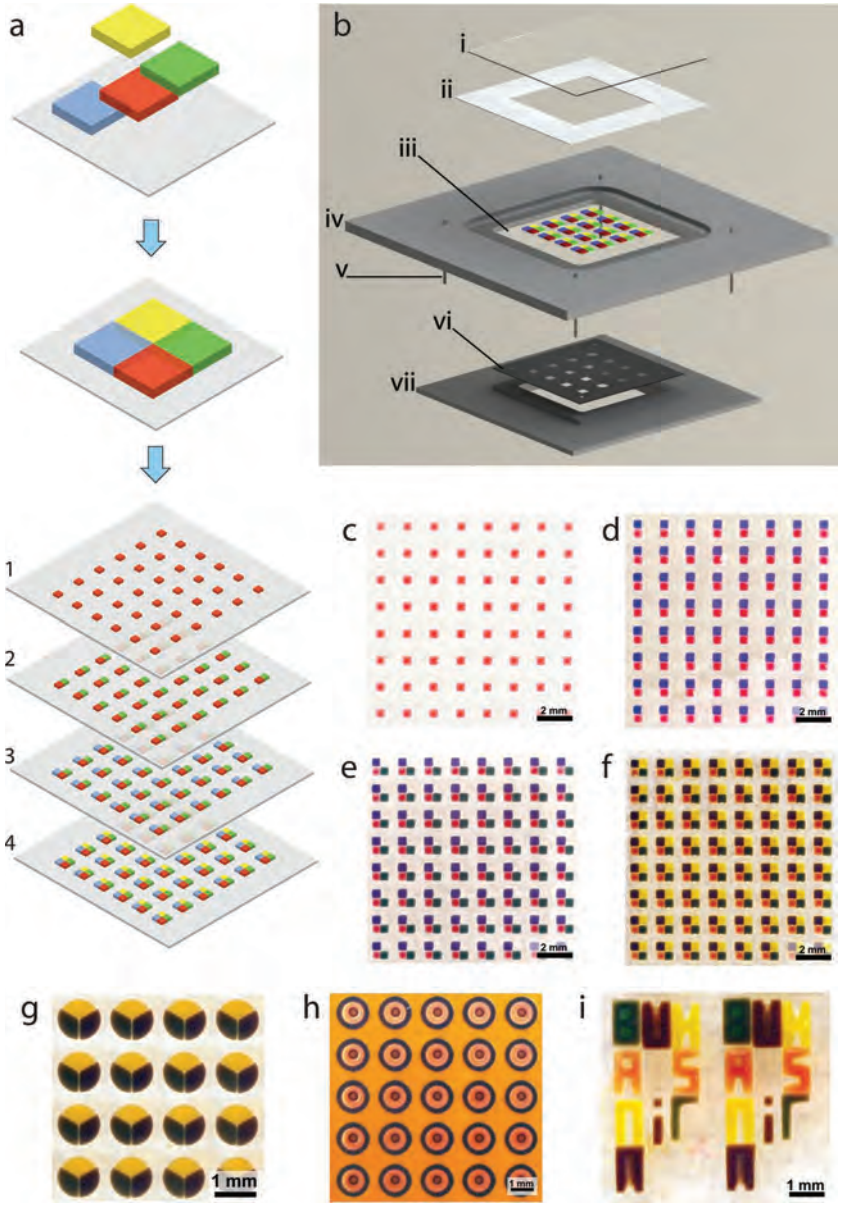

Figure 1. Digitally specified spatially heterogeneous microfabrication and tissue sculpting. (a) In this example, the tissue structure is composed of four different types of building blocks, each with specific cellular and ECM composition shown as different color codes. (b) Fabrication of 3D multilayer tissue prototypes via a layer-by-layer photomasking and alignment approach, with a series of photomasks, and a series of hydrogel solutions to be photocrosslinked to result in digitally sculpted hydrogels (e.g., containing different cell types, ECM components, and diffusible factors). The simple mask alignment and digital sculpting device comprises: (i) top cover slip of fabrication compartment, (ii) thickness control spacer, (iii) a treated glass cover slip on which the sculpted elements are immobilized, (iv) fabrication chamber, (v) alignment pins, (vi) predesigned photomask and (vii) mask holder that aligns on the fabrication chamber. Light is applied through the opening in mask holder. (c-f) Alignment and digital sculpting of individual elements is achieved using a photomask, which has digitally specified, engineered openings allowing photocrosslinking of tissue prototypes in a stepwise manner. Fabrication of cubic digitally sculpted blocks is demonstrated here. Radial circular (g), concentric circular (h) elements can also be sculpted, mimicking cross-section of embedded vasculature in a tissue construct, where yellow hydrogel encapsulates the three types of elements microfabricated as concentric circles. (i) Digital sculpting approach can also be used to generate complex structures such as microscale typescript (e.g., BWH, BAMM, HST, and MIT).

To overcome these challenges, thus addressing an unmet need in 3D tissue prototyping with microscale precision,[4,9,10,34] we created an optimized, inexpensive (~$50 material cost), and easy-to-use version of the powerful method used in semiconductor microfabrication,[35] multilayer photolithography, to build 3D digitally specified tissue constructs (**Figure 1**). The significance of the presented approach is that it is a scalable and generalizable biomanufacturing method with degrees of freedom in all three dimensions, with multiple-orders-of-magnitude lower cost compared to other specialized systems (e.g., stereolithography devices cost tens of thousands of dollars), and allows ~10 μm precision within and across layers offering an order-of-magnitude improvement over existing methods without requiring expensive lithographic aligners or computerized-stage microscopes. The key innovations include the strategy for photolithographically crosslinking hydrogels containing cells and ECM components using multiple masks with microscale control, to anchor them at specified coordinates in 3D space (by varying the cell and ECM compositions before the crosslinking step, we can modulate the biological and chemical materials being instantaneously incorporated into the engineered tissue as a function of time and space), as well as the very simple mechanical engineering strategies utilized: since we use simple alignment and layer-by-layer fabrication hardware, no specialized optics or alignment systems are needed for tissue fabrication, making our method eminently practicable in individual laboratories.

Using this platform, we developed a digitally specifiable 3D environment for brain cells, and explored the effect of 3D spatial confinement on neural cell survival and neurite growth. We further explored microscale engineered tissue complexity by developing prototype structures digitally sculpted with varying cellular composition (i.e., ESCs, HUVECs, and fibroblasts) and geometry (e.g., square, radially fractioned circular, and concentric circular), creating tissue prototypes with a high level of precision, versatility, flexibility, and scalability. Our work will support 3D, hierarchical, modular assembly of heterogeneous engineered tissues, advancing the synthetic biology-driven understanding of how tissues develop and change over time. This approach will also assist in meeting the clinical demand for replacement tissues and organs,[36] by enabling the service

ADVANCED MATERIALS
www.advmat.de

www.MaterialsViews.com

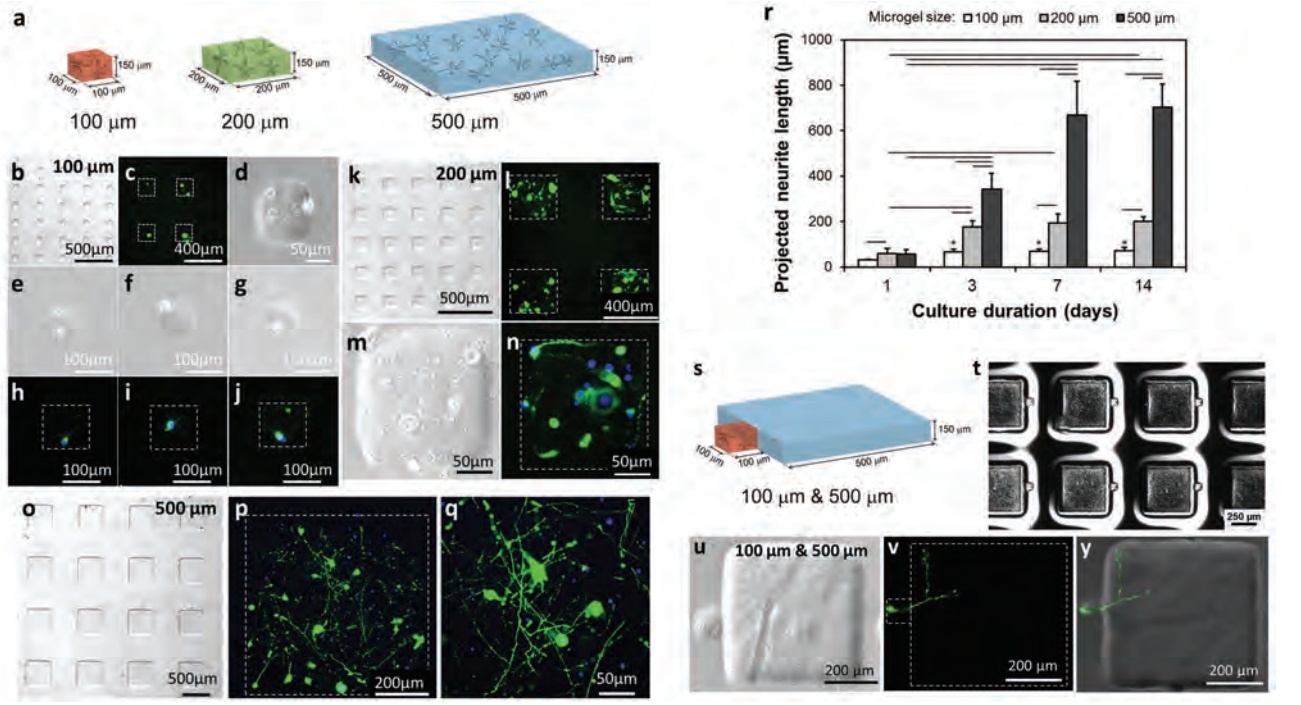

Figure 2. Digitally specified microfabricated neural tissue. (a) Primary neuron cells were inserted into 100 µm, 200 µm and 500 µm elements enabling visualization of neurite growth and development. Neurites (anti-Tau-1 staining in green) and nuclei (DAPI staining in blue) of neurons were observed in neural tissue constructs over 14 days of culture. (b–j) Neurons were digitally sculpted in 100 µm elements, (k–n) in 200 µm elements, and (o–q) in 500 µm elements. (r) Quantitative assessment of projected neurite length in digitally sculpted elements showed different growth dynamics of neurites over time in engineered constructs with different sizes. Horizontal lines connecting individual groups represent statistically significant difference and * represents statistically significant difference compared to 1 day culture ($p < 0.05$). Error bars represent mean ± STD (n = 3–6). (s) Digital sculpting of 100 µm tissue element next to a 500 µm tissue element, where only the 100 µm element includes neuron cell bodies. (t) Digitally sculpted array of adjacent 100 µm and 500 µm tissue prototypes. (u-y) Neuron cells in digitally sculpted 100 µm elements extended neurites into 500 µm elements. (The video in the Supporting Information shows 3D distribution of neuron cells and the neural circuit formed in digitally sculpted constructs).

of multiscale fabrication techniques in 3D, hierarchical, modular tissue design with broad applications.

We have developed an advanced fabrication process comprising a number of digitally controllable lithography steps (Figure 1a) to generate tissue complexity in 3D (Figure 1b). The geometry of each and every layer is tightly controlled by predesigned photolithography masks (Figure S1) to fabricate architectures and tissue prototypes composed of multiple building blocks (Figure 1c–f). We have shown that complexity and organization of the hydrogel architectures can be tightly controlled for various geometries, i.e., rectangular prism (Figure 1f), radially fractioned circular (radial circular) (Figure 1g), concentric circular (Figure 1h), and typescript (Figure 1i). The method utilizes a mask alignment setup (Figure 1b and S2) to achieve high alignment precision of the building blocks (Figure S3). We defined the alignment precision as the positioning repeatability of the centroid of the individual building blocks during microfabrication based on the computer aided design (Figure 1 and Figure S1). Alignment precision was determined (for details, see Supporting Information) to be within: 10.9 µm (±8.2) for square geometry; 11.2 µm (±4.5) for radial circular geometry; and 27.8 µm (±9.8) for concentric circular geometry (mean ± standard deviation (STD), n = 16–24 measurements for each geometry).

To demonstrate the utility of this digital tissue sculpting strategy, we assessed how neuron cell development and neurite growth could be studied in a space-constrained custom-tuned environment. We created digitally specified neural tissues made of lithographically specified hydrogel containing neonatal rat primary cortical neurons. We assessed neuron cell behavior in three different hydrogel sizes, each crafted lithographically as described (100 µm × 100 µm × 150 µm, 200 µm × 200 µm × 150 µm, 500 µm × 500 µm × 150 µm, **Figure 2**a). To morphologically assess neurons in engineered tissue prototypes, we performed labeling with anti-Tau-1 (axonal stain) and DAPI (nuclear stain), which clearly indicated the morphology of neurites and nuclei of the cells. In each 100 µm size element, only several neurons were encapsulated due to the space constraints, and the few cells exhibited short and undeveloped neurites (Figure 2b–j). We observed that neurons encapsulated in 200 µm (Figure 2k–n) and 500 µm (Figure 2o–q) elements formed more elaborate 3D geometries over comparable timescales (14 days in culture). Neurite (axon and dendrite) lengths were quantified under comparable photopolymerization conditions in different element sizes (Figure 2r). Specifically, neurons displayed longer neurites ($p < 0.05$, analysis of variance (ANOVA) with Tukey's posthoc test for multiple comparisons) in 200 µm elements compared to 100 µm elements, which demonstrated extremely

low growth. Neurons exhibited even longer neurites in 500 μm elements ($p < 0.05$). Neurite growth was observed in the first three days of culture in 100 μm and 200 μm elements, which reached a stagnant state after three days (Figure 2r). However, in 500 μm elements, neurite growth continued with a significant increase compared to day 1 and day 3 ($p < 0.05$) till day 7, after which a significant growth was no longer observed ($p > 0.05$). Projected neurite length was significantly greater ($p < 0.05$) in 500 μm elements than other size elements after 3 days of culture, which reached around 800 μm in length over 14 days in culture (Figure 2r). The distribution of neurons and their neurites in 3D was visualized using fluorescent confocal imaging (see video in the Supporting Information). We did not observe any difference in cell survival or morphology in different sections of the engineered constructs in 3D.

The above results suggested that neuronal growth is regulated by available volume. But larger volume tissue cubes also contained greater numbers of neurons. Ideally one would be able to examine effects of volume, and even 3D shape, on neural growth, independent of cell density. Our technology enables such assessments of pure geometrical influences on neuron growth, here demonstrated by our fabrication of complex tissue structures with a 100 μm element touching a 500 μm element (Figure 2s) in an array (Figure 2t). In this configuration, we selectively encapsulated single neuron cells in the 100 μm element, as enabled by our selective photolithography, to investigate the growth of the cell whose body is localized to a confined structure, but for which neurites are allowed to grow into a larger environment. During the 14 day culture period, single neuron cells spatially positioned in 100 μm elements were observed to grow towards the 500 μm element and extend neurites towards the larger gel, resulting in a projected neurite length of 507 μm (±103, STD, $n = 7$) (Figure 2u–y). Indeed, such long neurites extending into the larger 3D hydrogel compartment were observed in all the sculpted structures analyzed ($n = 7$), suggesting that the neurite growth is not only dependent on the number of cells encapsulated in a 100 μm element, but is a function of the complex geometry of spatial confinement. Neurons appeared to be responsive to their surroundings in a novel way, showing how our technology enables the probing of parameters important for developmental as well as tissue engineering studies.

To gain insight into the cellular composition of the 3D neural tissue prototypes, we identified neuronal and glial populations by staining for Tau-1 and GFAP (**Figure 3**a–i). The numbers of neuronal and glial cells were statistically similar ($p > 0.05$, non-parametric Mann-Whitney U test) (Figure 3j), displaying a ratio reminiscent of natural brain tissue.[37] We observed both CaMKII- and GAD65-positive neurons indicating that both excitatory and inhibitory neural cells were present in the 3D neural tissue prototypes (Figure 3d–i). Excitatory neurons constituted the majority of the neurons, amounting to 83.9% (±12.6, STD; $n = 5$) of the total number of neurons, similar to the fraction (i.e., 4:1 ratio of excitatory to inhibitory) of cortical neurons in vivo that are excitatory.[38] Our results suggested that neural networks in elements comprised a complex population of brain cells, including excitatory neurons, inhibitory neurons, and glial cells, appearing at comparable ratios to that in the native rodent cortex, and highlighting the power of our technology to preserve a diversity of brain cell types.

Photopolymerizable polymers and hydrogels (e.g., poly(ethylene glycol)/poly(L-lysine), chitosan) have been used in combination with primary neurons, neural stem and progenitor cells for neural tissue engineering and neural cell delivery applications.[30,39–41] In the current study, in which we extended the power of photopolymerizable hydrogels by 3D digital tissue sculpting, we accordingly validated the method with neuron cell viability studies. We evaluated the effects of the duration and intensity of ultraviolet (UV) light exposure to create photopolymerizable gelatin methacrylate hydrogels encapsulating primary neuron cells. We first assessed the effect of light exposure duration (20, 30, and 60 s at 2.9 mW/cm^2) on cell viability (Figure 3k–m). We observed that neurons were viable after 30 seconds of light exposure applied during microfabrication. The viabilities were observed to be 85.54 ± 7.15%, 76.10 ± 12.22%, and 22.33 ± 3.64% at 20, 30, and 60 s, respectively ($n = 3$–8 samples of each kind). Sixty seconds of exposure resulted in significantly less ($p < 0.05$) cell viability compared to 20 and 30 seconds (Figure 3k). Therefore, results indicated that less than 30 seconds had minimal effect ($p < 0.05$) on neurons with a higher viability compared to 60 s of light exposure. Next, we assessed the effect of UV light intensity (2.9–6.9 mW/cm^2 for 20 s) on cell viability in neuron encapsulating elements (Figure 3l). We observed no statistically significant effect ($p > 0.05$, $n = 3$) on cell viability as a result of increasing intensity. The neuron cell viability was 83.35 ± 2.22% at an intensity of 6.9 mW/cm^2. To achieve high cell viability and minimize potential effects of UV light, we used 2.9 mW/cm^2 intensity and 20 seconds crosslinking duration, which resulted in a viability of 85.54 ± 7.15%, not significantly different compared to controls that were not exposed to light (89.24 ± 3.84%; $p > 0.05$; $n = 3$ photocrosslinked cubes, $n = 3$ control samples). Cell viability assays were conducted at different time points (Figure 3m): day 0 (immediately after photocrosslinking at 2.9 mW/cm^2 intensity and 20 seconds crosslinking duration), day 3 (after 3 days of culture) and day 10. We observed similar ($p > 0.05$, n = 3–8) cell viabilities at day 3 (82.82 ± 8.23%) and day 10 (89.80 ± 5.26%) compared to day 0 (85.54 ± 7.15%). These results demonstrated that the photopolymerization parameters of photocrosslinkable hydrogels have minimal effect on neural cell viability both in short and long term.

To demonstrate the ability to digitally sculpt complex tissues with multiple cell types, we next created engineered 3D tissue constructs (Figure 3n) composed of three cell types (Figure 3o), encapsulating ESCs, HUVECs and NIH 3T3 fibroblasts mimicking the complexity in studies aiming to regenerate myocardium.[42] We observed that each cell type was spatially confined in individual elements, as indicated by cell tracker staining (Figure 3o). We have shown that cellular composition as well as cellular concentration in each building block can be controlled spatially (Figure 3o,p). We also observed that cells were viable in tissue prototypes after microfabrication (Figure 3p). The quantitative viability analysis showed that all cell types remained viable at the end of three day in vitro culture: 92% (±5%), 74% (±8%), and 95% (±3%) for ESCs, and 3T3s, and HUVECs, respectively (Figure 3q).

To demonstrate the 3D tissue sculpting capability of the method, we created multiple layer 3D tissue constructs

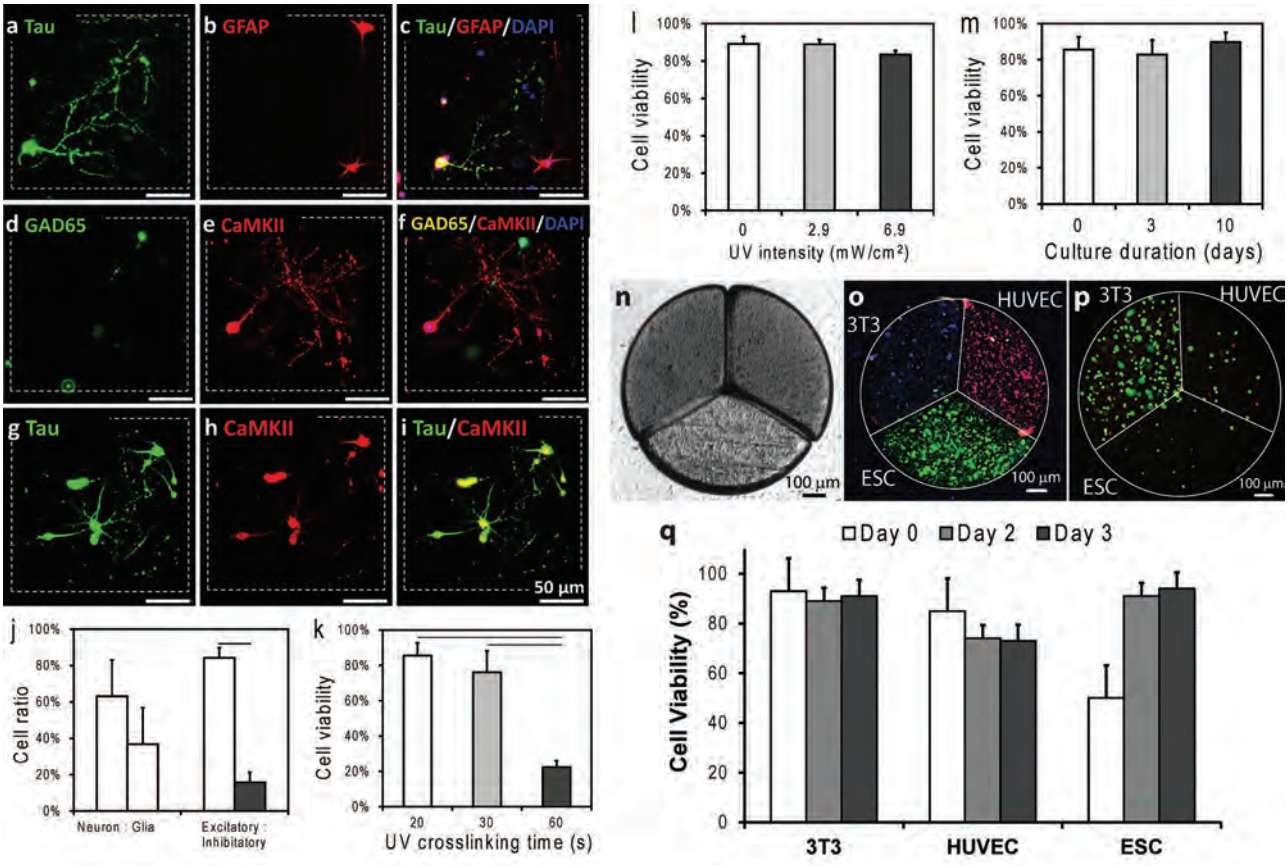

Figure 3. Immunofluorescent labeling of neurons, glia, excitatory, and inhibitory cells and multicell-type tissue prototypes generated using digitally specified tissue engineering. (a–c) Anti-Tau-1 labeled neurons (green), anti-GFAP labeled glial cells (red), and merged image is shown (DAPI in blue). (d–f) Anti-GAD65 labeled inhibitory neurons (green), anti-CaMKII labeled excitatory neurons (red), and merged image is shown (DAPI in blue). (g,h) Tau-1-positive label (green) and CaMKII-positive label (red), and merged image. Scale bars represent 50 μm of length. Dashed squares represent the borders of digitally specified 3D neural tissue constructs. (j) Quantitative plot showing the cell type ratio in hydrogels after 3 weeks of culture. Anti-Tau-1 for neurons (63.16 ± 19.92%), anti-GFAP for glia (36.84 ± 19.92%); anti-CaMKII for excitatory neurons (84.20 ± 10.96%), anti-GAD65 for inhibitory neurons (15.80 ± 10.96%) (n = 4–5). (k) UV light exposure of up to 30 seconds did not significantly affect neuron cell viability ($p > 0.05$). (l) Light intensity did not have a statistically significant effect on neuron cell viability. (m) Neuron viability was observed in tissue prototypes up to 10 days in culture n = 3–8). (n) Light microscope image of digitally sculpted radially fractioned circle with three different cell types. (o) Encapsulation of three cell types (ESCs in green, 3T3 cells in blue, HUVECs in red) in a single tissue prototype (10^6 cells/mL for all cell types). Cells were stained using cell tracker dyes to display their distribution after microfabrication. (p) Encapsulation of three cell types in varying concentrations using digital sculpting method: ESCs (0.5×10^6 cells/mL), HUVEC (0.75×10^6 cells/mL) and 3T3 (10^6 cells/mL). Live/dead stained cells after digital sculpting (green: live cells, red: nonviable cells). (q) Cells remained highly viable at the end of three day in vitro culture in digitally specified tissue constructs: 92% (±5%), 74% (±8%), and 95% (±3%) for ESCs, and 3T3s, and HUVECs, respectively (n = 3–7). Error bars represent mean ± STD of the mean. Horizontal lines in the plots (j and k) connecting individual groups represent statistically significant difference ($p < 0.05$).

(**Figure 4**). In this multilayer fabrication process, after the first layer fabrication, the lithography process is repeated to create a second and then a third layer (Figure 4a). In this process, compositions of each element were alternated in different layers to increase the degree of complexity achievable. With this process, large number of complex multilayer structures can be fabricated simultaneously (Figure 4b), in various geometries and architecture (Figure 4c-i), indicating the high throughput potential of this manufacturing platform. The same system and approach would be simply scaled up in size to achieve millions of tissue prototypes. For instance, with a standard 12 inch mask used in the semiconductor industry, 145 thousand tissue prototypes with an element size of 400 μm and separation of 400 μm can be fabricated. This number increases to 2.3 million tissue prototypes with an element size of 100 μm and a separation of 100 μm using the presented process with a 12 inch mask. Thus, our technology advances the scales of fabrication in engineering complex tissue architectures.

The multilayer photolithography digital sculpting method presented here utilizes multiple masks to create individual elements in a tissue construct (Figures S1 and S2). Since the masks have designated openings to create individual elements in a layer, the cells in an individual element are exposed to light only once during the fabrication of a layer. On the other hand, photocrosslinked hydrogels have been commonly used in the literature to encapsulate various cells, including neural cells,[43] for applications in tissue engineering.[44,45] Potential effects of UV on cells during the fabrication process of photocrosslinked

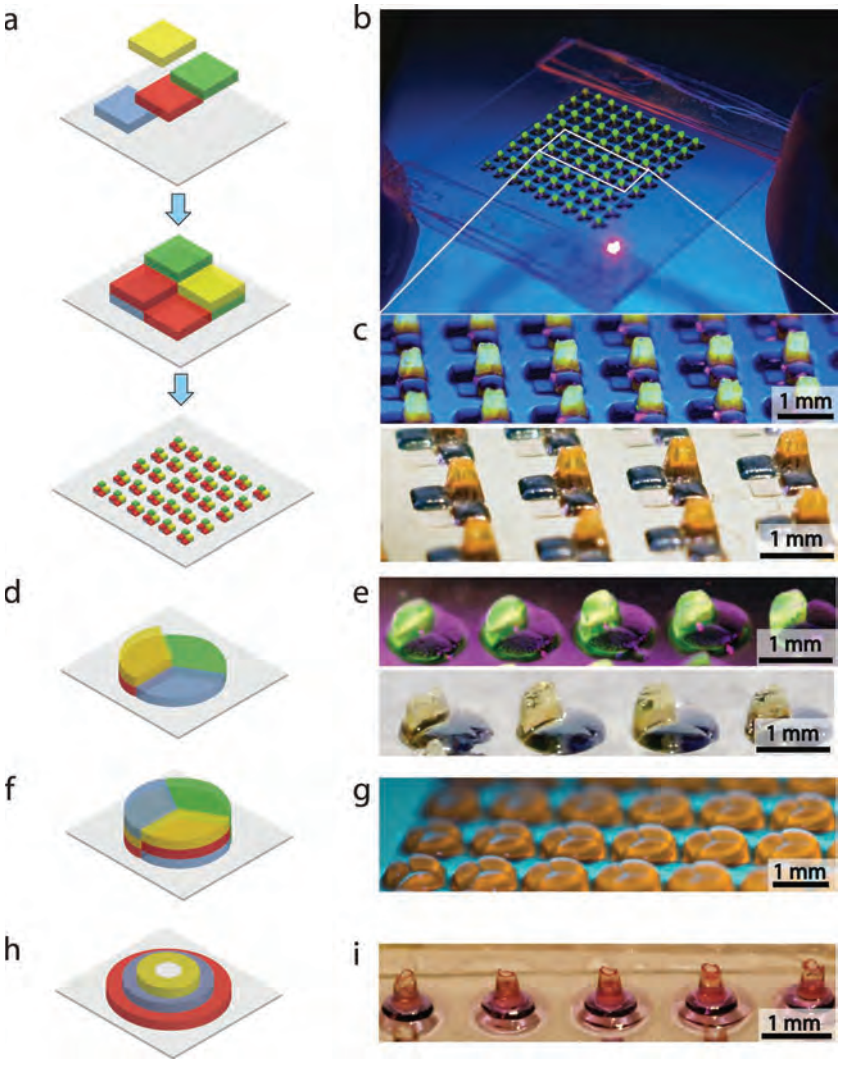

Figure 4. Multilayer 3D digitally specified spatially heterogeneous tissue sculpting. (a) Fabrication of 3D square geometry tissue prototypes using multilayer photolithography. (b,c) Microfabricated array of multilayer digitally specified 3D tissue prototypes. (d–g) Side view of 3D digitally sculpted spatially heterogeneous radial circular tissue construct at different stages of microfabrication. (h,i) Side view of three layered concentric circular microfabricated tissue construct.

materials can be eliminated by replacing the UV light source with a visible light source and utilizing visible light photoinitiators, such as eosin-Y, triethanolamine, or camphorquinone as reported earlier.[46–49]

In this work, we have demonstrated the compatibility of our digital tissue sculpting technology with neural cells. To achieve this, we developed digitally specifiable 3D hydrogel scaffolds that can be used as neural cell carriers, which supported neural cell survival and development with a naturalistic ratio of multiple cell-types. The engineered neural tissue presented here offers new opportunities as a platform technology for 3D in vitro studies of neural networks. Further, the in situ engineered neural tissue may enable broad clinical applications for engineering neural implants, providing an important step forward in transplantation and cell therapy for neural degenerative diseases, as well as injuries of brain and spinal cord. In combination with optogenetic methods for activating defined cell types,[50] as well as robotic methods for analyzing single neurons in intact tissues in an integrative fashion,[51] the described methodologies may open up neural tissue engineering to the regime of highly accurate 3D architectures capable of exhibiting naturalistic cell type distributions. With this system, long-term culture studies of neurons may be performed, which enable gaining insight to neuronal and neurite development in precisely controlled geometries. Importantly, these new insights and the digitally specifiable neural tissue could act as testbeds that can lead to disruptive advances such as bioengineered brain with a natural diversity of neuron types that would enable restoration of brain function after neurodegeneration, stroke, traumatic brain injury, spinal cord injury, or amyotrophic lateral sclerosis.

We digitally sculpted multiple cell types in elements within a single tissue prototype in a high throughput and repeatable manner. This method is based on multilayer photolithography used in the semiconductor industry and presents great potential to become a broadly applicable method for high-throughput applications in tissue engineering, regenerative medicine, and pharmacological studies. This photolithographic approach enables digital modulation of biological and chemical materials being instantaneously incorporated into the engineered architecture as a function of time and space allowing microscale precision without requiring specialized optics or robotics. This advancement allows us to envision building millions of digitally specified tissue prototypes with predetermined biomaterials, encapsulated molecules and cell types at complexity and throughput levels not attained before for in vitro cultures. The developed method would become a broadly enabling platform for studying cell–cell and cell-matrix interactions in a variety of physiologic (e.g., stem cell differentiation) and pathological (e.g., cancer) settings, in vitro drug screening applications in pharmaceutical industry, and in advanced biomanufacturing.

Supporting Information

Supporting Information is available from the Wiley Online Library or from the author.

Acknowledgements

This work was performed at Demirci Bio-Acoustic MEMS in Medicine (BAMM) Laboratories at the Division of Biomedical Engineering at Brigham and Women's Hospital, Harvard Medical School. Dr. Demirci

acknowledges that this material is based in part upon work supported by the NSF CAREER Award Number 1150733, NIH R21-HL112114 and R21-AI087107. ESB was supported by the Paul Allen Family Foundation, New York Stem Cell Foundation, NIH, NSF, the IET AF Harvey Prize, and MIT Lincoln Laboratory.

Received: August 8, 2012
Revised: October 4, 2012
Published online: November 27, 2012

[1] F. Pampaloni, E. G. Reynaud, E. H. K. Stelzer, *Nat. Rev. Mol. Cell Biol.* **2007**, *8*, 839.
[2] K. M. Yamada, E. Cukierman, *Cell* **2007**, *130*, 601.
[3] H. Geckil, F. Xu, X. Zhang, S. Moon, U. Demirci, *Nanomedicine (Lond)* **2010**, *5*, 469.
[4] U. A. Gurkan, S. Tasoglu, D. Kavaz, M. C. Demirel, U. Demirci, *Adv. Healthcare Mater.* **2012**, *1*, 149.
[5] S. Moon, S. K. Hasan, Y. S. Song, F. Xu, H. O. Keles, F. Manzur, S. Mikkilineni, J. W. Hong, J. Nagatomi, E. Haeggstrom, A. Khademhosseini, U. Demirci, *Tissue Eng. Part C Methods* **2010**, *16*, 157.
[6] Y. S. Song, R. L. Lin, G. Montesano, N. G. Durmus, G. Lee, S. S. Yoo, E. Kayaalp, E. Haeggstrom, A. Khademhosseini, U. Demirci, *Anal. Bioanal. Chem.* **2009**, *395*, 185.
[7] M. Anghelina, P. Krishnan, L. Moldovan, N. I. Moldovan, *Am. J. Pathol.* **2006**, *168*, 529.
[8] C. Chuong, P. Wu, M. Plikus, T. Jiang, R. Bruce Widelitz, P. S. Gerald, in *Current Topics in Developmental Biology*, Vol. Volume *72*, Academic Press, **2005**, 237.
[9] F. Xu, T. D. Finley, M. Turkaydin, Y. Sung, U. A. Gurkan, A. S. Yavuz, R. O. Guldiken, U. Demirci, *Biomaterials* **2011**, *32*, 7847.
[10] F. Xu, C. A. Wu, V. Rengarajan, T. D. Finley, H. O. Keles, Y. Sung, B. Li, U. A. Gurkan, U. Demirci, *Adv. Mater.* **2011**, *23*, 4254.
[11] E. Ceyhan, F. Xu, U. A. Gurkan, A. E. Emre, E. S. Turali, R. El Assal, A. Acikgenc, C.-a. M. Wu, U. Demirci, *Lab Chip* **2012**.
[12] S. Moon, E. Ceyhan, U. A. Gurkan, U. Demirci, *PLoS ONE* **2011**, *6*, e21580.
[13] S. Tasoglu, D. Kavaz, U. A. Gurkan, S. Guven, P. Chen, R. Zheng, U. Demirci, *Adv. Mater.* **2012**, DOI10.1002/adma201200285.
[14] E. E. Hui, S. N. Bhatia, *Proc. Natl. Acad. Sci. USA* **2007**, *104*, 5722.
[15] L. G. Griffith, M. A. Swartz, *Nat. Rev. Mol. Cell Biol.* **2006**, *7*, 211.
[16] A. Birgersdotter, R. Sandberg, I. Ernberg, *Sem. Cancer Biol.* **2005**, *15*, 405.
[17] U. Gurkan, V. Kishore, K. Condon, T. Bellido, O. Akkus, *Calcified Tissue Int.* **2011**, *88*, 388.
[18] E. Lavik, *Neural Tissue Engineering*, Springer, New York **2011**.
[19] K. Musick, D. Khatami, B. C. Wheeler, *Lab Chip* **2009**, *9*, 2036.
[20] J. Silver, J. H. Miller, *Nat. Rev. Neurosci.* **2004**, *5*, 146.
[21] D. H. Kim, J. Viventi, J. J. Amsden, J. L. Xiao, L. Vigeland, Y. S. Kim, J. A. Blanco, B. Panilaitis, E. S. Frechette, D. Contreras, D. L. Kaplan, F. G. Omenetto, Y. G. Huang, K. C. Hwang, M. R. Zakin, B. Litt, J. A. Rogers, *Nat. Mater.* **2010**, *9*, 511.
[22] R. G. Wylie, S. Ahsan, Y. Aizawa, K. L. Maxwell, C. M. Morshead, M. S. Shoichet, *Nat. Mater.* **2011**, *10*, 799.
[23] V. Chan, P. Zorlutuna, J. H. Jeong, H. Kong, R. Bashir, *Lab Chip* **2010**, *10*, 2062.
[24] J. C. Culver, J. C. Hoffmann, R. A. Poché, J. H. Slater, J. L. West, M. E. Dickinson, *Adv. Mater.* **2012**, *24*, 2344.
[25] J. S. Miller, K. R. Stevens, M. T. Yang, B. M. Baker, D.-H. T. Nguyen, D. M. Cohen, E. Toro, A. A. Chen, P. A. Galie, X. Yu, R. Chaturvedi, S. N. Bhatia, C. S. Chen, *Nat. Mater.* **2012**, *11*, 768.
[26] R. P. Visconti, V. Kasyanov, C. Gentile, J. Zhang, R. R. Markwald, V. Mironov, *Expert. Opin. Biol. Ther.* **2010**, *10*, 409.
[27] A. Khademhosseini, R. Langer, J. Borenstein, J. P. Vacanti, *Proc. Natl. Acad. Sci. USA* **2006**, *103*, 2480.
[28] X. Wang, Y. Yan, R. Zhang, *Tissue Eng Part B Rev* **2010**, *16*, 189.
[29] C. M. Smith, A. L. Stone, R. L. Parkhill, R. L. Stewart, M. W. Simpkins, A. M. Kachurin, W. L. Warren, S. K. Williams, *Tissue Eng* **2004**, *10*, 1566.
[30] J. L. Curley, M. J. Moore, *J. Biomed. Mater. Res. Part A* **2011**, *99A*, 532.
[31] V. L. Tsang, A. A. Chen, L. M. Cho, K. D. Jadin, R. L. Sah, S. DeLong, J. L. West, S. N. Bhatia, *FASEB J.* **2007**, *21*, 790.
[32] P. Zorlutuna, J. H. Jeong, H. Kong, R. Bashir, *Adv. Funct. Mater.* **2011**, *21*, 3642.
[33] F. Xu, S. J. Moon, A. E. Emre, E. S. Turali, Y. S. Song, S. A. Hacking, J. Nagatomi, U. Demirci, *Biofabrication* **2010**, *2*, 014105.
[34] F. Xu, J. Wu, S. Wang, N. G. Durmus, U. A. Gurkan, U. Demirci, *Biofabrication* **2011**, *3*, 034101.
[35] G. E. Moore, *Proc. IEEE* **1998**, *86*, 82.
[36] R. J. Davenport, *Science* **2005**, *309*, 84.
[37] N. J. Allen, B. A. Barres, *Nature* **2009**, *457*, 675.
[38] H. Markram, M. Toledo-Rodriguez, Y. Wang, A. Gupta, G. Silberberg, C. Wu, *Nat. Rev. Neurosci.* **2004**, *5*, 793.
[39] S. Royce Hynes, L. M. McGregor, M. Ford Rauch, E. B. Lavik, *J. Biomater. Sci. Polym. Ed.* **2007**, *18*, 1017.
[40] S. R. Hynes, M. F. Rauch, J. P. Bertram, E. B. Lavik, *J. Biomed. Mater. Res. Part A* **2009**, *89*, 499.
[41] C. M. Valmikinathan, V. J. Mukhatyar, A. Jain, L. Karumbaiah, M. Dasari, R. V. Bellamkonda, *Soft Matter* **2012**, *8*, 1964.
[42] G. Condorelli, U. Borello, L. De Angelis, M. Latronico, D. Sirabella, M. Coletta, R. Galli, G. Balconi, A. Follenzi, G. Frati, M. G. Cusella De Angelis, L. Gioglio, S. Amuchastegui, L. Adorini, L. Naldini, A. Vescovi, E. Dejana, G. Cossu, *Proc. Natl. Acad. Sci. USA* **2001**, *98*, 10733.
[43] E. R. Aurand, K. J. Lampe, K. B. Bjugstad, *Neurosci. Res.* **2012**, *72*, 199.
[44] D. Seliktar, *Science* **2012**, *336*, 1124.
[45] S. J. Bryant, C. R. Nuttelman, K. S. Anseth, *J. Biomater. Sci. Polym. Ed.* **2000**, *11*, 439.
[46] G. M. Cruise, D. S. Scharp, J. A. Hubbell, *Biomaterials* **1998**, *19*, 1287.
[47] G. M. Cruise, O. D. Hegre, F. V. Lamberti, S. R. Hager, R. Hill, D. S. Scharp, J. A. Hubbell, *Cell Transplant* **1999**, *8*, 293.
[48] T. A. Ahmed, M. Griffith, M. Hincke, *Tissue Eng.* **2007**, *13*, 1469.
[49] G. D. Nicodemus, S. J. Bryant, *Tissue Eng. Part B Rev.* **2008**, *14*, 149.
[50] E. S. Boyden, *F1000 Biol. Rep.* **1000**, *3*, 3.
[51] S. B. Kodandaramaiah, G. T. Franzesi, B. Y. Chow, E. S. Boyden, C. R. Forest, *Nat. Methods* **2012**, *9*, 585.

ADVANCED MATERIALS

Supporting Information

for *Adv. Mater.*, DOI: 10.1002/adma.201203261

Simple Precision Creation of Digitally Specified, Spatially Heterogeneous, Engineered Tissue Architectures

Umut Atakan Gurkan, Yantao Fan, Feng Xu, Burcu Erkmen, Emel Sokullu Urkac, Gunes Parlakgul, Jacob Bernstein, Wangli Xing, Edward S. Boyden,* and Utkan Demirci**

Submitted to ADVANCED MATERIALS

DOI: 10.1002/adma.201203261

Supporting Information

Simple precision creation of digitally specified, spatially heterogeneous, engineered tissue architectures

By Umut Atakan Gurkan, Yantao Fan, Feng Xu, Burcu Erkmen, Emel Sokullu Urkac, Gunes Parlakgul, Jacob Bernstein, Wangli Xing, Edward S. Boyden*, and Utkan Demirci**

Dr. U. A. G. Author-One, Y. F. Author-One, Dr. F. X. Author-Two, B. E. Author-Three, Dr. E. S. U. Author-Four, G. P. Author-Five
Harvard Medical School, Brigham and Women's Hospital
Harvard-MIT Health Sciences & Technology
65 Landsdowne St. PRB 252
Cambridge, MA 02139, USA

J. B. Author-Six
Media Lab and McGovern Institute, Departments of Brain and Cognitive Sciences and Biological Engineering, Massachusetts Institute of Technology,
Cambridge, Massachusetts 02139, USA

[*] Dr. W. X., Corresponding-Author
Medical Systems Biology Research Center, School of Medicine, Tsinghua University, Beijing 100084, PR China
National Engineering Research Center for Beijing Biochip Technology, 18 Life Science Parkway, Beijing, 102206, PR China

[*] Dr. E. S. B., Corresponding-Author
Media Lab and McGovern Institute, Departments of Brain and Cognitive Sciences and Biological Engineering, Massachusetts Institute of Technology,
Cambridge, Massachusetts 02139, USA
E-mail: edboyden@mit.edu

[*] Dr. U. D. Corresponding-Author
Harvard Medical School, Brigham and Women's Hospital
Harvard-MIT Health Sciences & Technology
65 Landsdowne St. PRB 252
Cambridge, MA 02139, USA
E-mail: udemirci@rics.bwh.harvard.edu

Keywords: three-dimensional microfabrication, biomanufacturing, biofabricatiom, advanced manufacturing, tissue engineering, neural engineering

Individual masks were designed for each colored section of the overall geometry which are referred to as elements of the digitally fabricated geometries. Masks were created using AutoCAD (AutoCAD, v2012, Autodesk Inc., CA), for 5 different geometries (square, concentric circles, radially fractioned circles, two consecutive squares with dimensions: 100 μm by 100 μm; 500 μm by 500 μm, and microscale script (BWH, BAMM, HST, MIT) (**Fig. s1**). Within each geometry, to create each of elements, different set of masks were designed. The number of masks for each geometry equaled the number of elements it has and each mask was labeled on top with a letter and a number that represents the geometry and the element, respectively. Every mask was designed such that when aligned on top of each other they would create consecutive or concentric shapes. Alignment of the masks with the mask holders was achieved through 4 reference points that are located at each corner of the mask and separated by 16 mm. The black frame in the mask was designed to be 15 mm by 15 mm.

To ensure precision in the alignment of the individual units of the digitally sculpted tissue prototypes, a dual system of holders for the mask and the coverslip were designed and fabricated. Masks were created for each element of a specific geometry were placed on separate holders and the four reference dots on them were aligned with the holes of the holder (**Fig. s2**) under a stereomicroscope (Leica Microsystems Inc., Buffalo Grove, IL). This alignment provided the basis for maintaining the desired precision. The distance between any two reference dots was 16mm. The labels on each mask were used to maintain consistency throughout the fabrication of the elements. Between the steps of fabricating each element, when the masks were swapped, each label was oriented towards a mark that was placed on the cover slip holder. A TMSPMA coated cover slip was placed in the holder and stabilized with a low- viscosity adhesive (Loctite 420 Instant Adhesive Wicking Grade, Henkel). Stabilizing the coated coverslip is significant in maintaining the precision in the alignment of each element. Once stabilized, a space of 150μm was created with a glass slide spacer (**Fig. s2**).

The alignment posts were used to align and keep the setup stable during the fabrications process. Once the masks were aligned on the mask holder the following procedure was followed for fabrication:

I. The first element of the tissue prototype was fabricated by pipetting 50 μL of the hydrogel precursor solution on to the 3-(trimethoxysilyl) propylmethacrylate (TMSPMA) (Sigma-Aldrich, St. Louis, MO, USA) coated glass slide which was then covered with a secondary coverslip (**Fig. 1 and Fig. s2**). In the case where a thicker shape was created as in the case of multilayer fabrication (300 μm height), 100 μL of hydrogel precursor solution was pipetted on to the coverslip.

II. The mask holder was placed on top of the coverslip holder and both were connected through the alignment posts. In this configuration, the mask was placed directly above the TMSPMA coated coverslip, allowing the cross-linked hydrogels to attach to the coated coverslip.

III. The setup was placed under the UV light using The Omnicure® S2000 UV/Visible Spot Curing System (EXPO Photonic Inc., Ontario, Canada). Mask holder side was oriented up, and the system was exposed to light from a distance of 35 mm. The power density was set to be 3.6 mW/cm² during the fabrication of colored tissue prototypes and at 2.5 mW/cm² for cell encapsulating tissue prototypes. The duration of the exposure varied according to the color of the hydrogel solution (**Table s1**).

IV. As the final step, the top coverslip was removed and the uncross-linked hydrogel precursor solution was washed away with PBS.

V. To fabricate the second element of tissue prototype, a second precursor solution was added to the same TMSPMA coated coverslip and was again covered with a second coverslip along with the first elements of the tissue prototype. The mask holder with the second mask (**Fig. s1**) was then placed on top of the coverslip holder and similarly,

was exposed to UV light. This process was repeated to get the desired tissue prototype. At the end of this process, a tissue prototype composed of digitally specified elements was fabricated (**Fig. 1**). The fabricated tissue prototype containing Procion MX dyes (Sigma-Aldrich, St. Louis, MO, USA) were imaged both with a camera (Sony, DSLR A700) and an inverted microscope (Nikon TE2000).

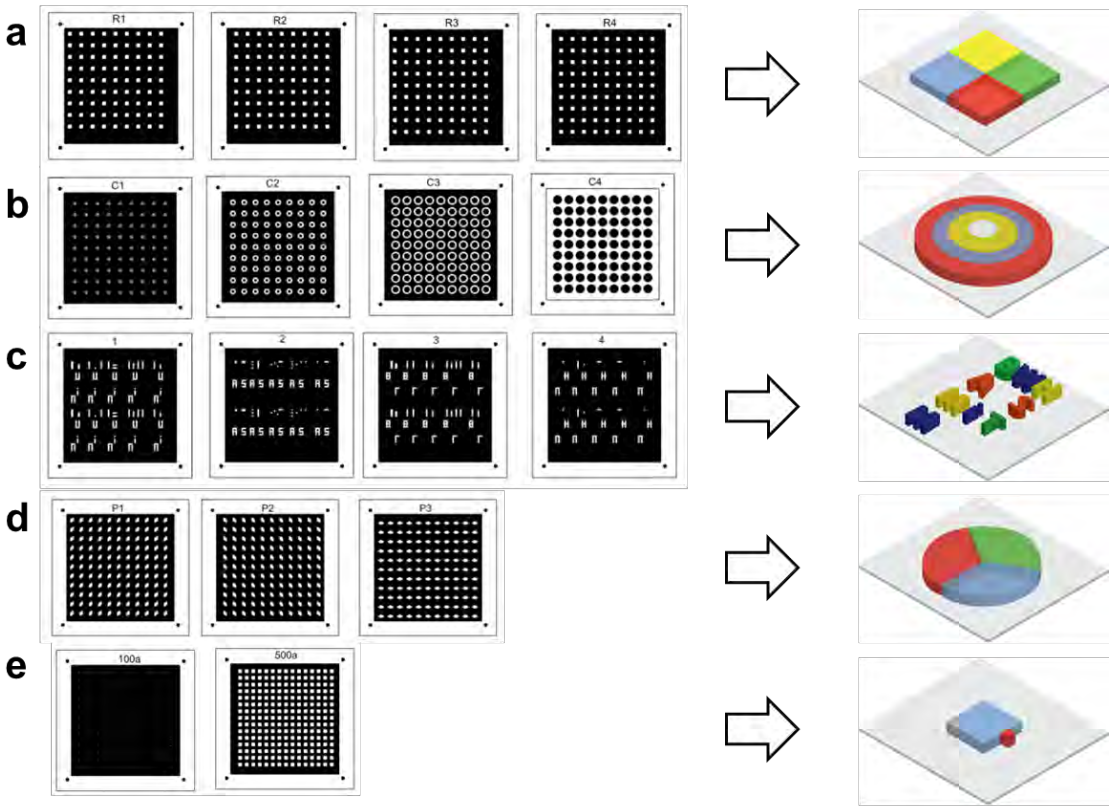

Figure s1: Masks were designed using computer aided design software to create digitally sculpted tissue constructs in a stepwise fashion. Steps and shapes were represented by the numbers printed on the masks (ii) (A) 4 masks were created for the square geometry by shifting each mask by 500 μm in up, down and side orientation. (B) 4 masks were created for the concentric circle geometry with diameters 200 μm, 400 μm, 800 μm, and 1200 μm. The fourth mask was designed to surround the three concentric circles and represent the surrounding tissue. (C) 4 masks were designed to create a micro-scale printed script (BWH, BAMM, HST, and MIT). The width and height of a letter within the script were 600 μm and 1000 μm respectively. (D) 3 masks were designed to create 120° sections of a pie chart with a diameter of 1000 μm. (E) A 100 μm by 100 μm square mask and a 500 μm by 500 μm square mask were aligned to have tangential contact.

To microfabricate neuron encapsulating tissue prototypes, three kinds of photomasks were designed with arrays of 100 × 100 μm, 200 × 200 μm and 500 × 500 μm squares. The

schematic illustration of this fabrication process is shown in **Fig. 1**. We used a spacer height of 150 μm, resulting in elements with dimensions of 100 × 100 × 150 μm, 200 × 200 × 150 μm and 500 × 500× 150 μm (**Fig. 2a**). To fabricate neuron encapsulating elements, 50 μL of neuron-suspended hydrogel (GelMA) precursor solution (*i.e.* 5 % (w/v) GelMA and 0.5 % (w/v) Irgacure 2959 photoinitiator) with 5×10^6 cells/mL was pipetted onto a polystyrene substrate. A TMSPMA modified glass slide was used (**Fig. s2e**). The photomask was then placed on the TMSPMA glass slide and exposed to UV light (**Fig. s2e**). The cover slide was washed with PBS to remove excess precursor solution. At the end of the microfabrication process, the constructs were placed in a 6-well plate for culture. Two photocrosslinking parameters (intensity and exposure duration) were optimized to fabricate neuron encapsulating tissue constructs (**Fig. 3k&l**). To assess UV intensity effect on cell viability, we used 6.9 mW/cm^2 and 2.9 mW/cm^2 intensities at UV exposure duration of 20 seconds. We also tested three different exposure durations of 20, 30, and 60 seconds (at an intensity of 2.9 mW/cm^2). After crosslinking and PBS washing steps, neuron encapsulating elements were stained with a live/dead assay. We have also employed the digitally specified tissue prototype fabrication to engineered a neuron cell encapsulating tissue composed of a 100 × 100 × 150 μm and a 500 × 500× 150 μm element (**Fig. 2s-y**).

The process to fabricate single-layer multi-element hydrogels was repeated to fabricate 3D multilayer prototypes via a layer-by-layer approach mimicking that in the semiconductor processing to build multilayer structures. Multiple glass slide layers (150 μm thick for each layer) were added in the base part to achieve the desired height and thickness for the multiple layers. For instance, the first layer of tissue prototypes was fabricated with a 150 μm thick base, and in order to fabricate the second layer, another glass slide layer of 150 μm was placed on top of the previous, giving the second layer a thickness of 300 μm in total (**Fig. 1**). After crosslinking, uncross-linked hydrogel precursor solution was washed away with PBS.

Another gel solution was then pipetted and crosslinked. The second layer was fabricated on the top of the first layer with a 300 µm thick base, while the third layer was fabricated on the top of the second layer with a 450 µm thick base. Then, we obtained three-layer tissue prototypes with 150 µm thick layers. To better observe and image the multiple layers, the glass slide layers of thickness 150µm were doubled for each layer giving them each a thickness of 300µm.

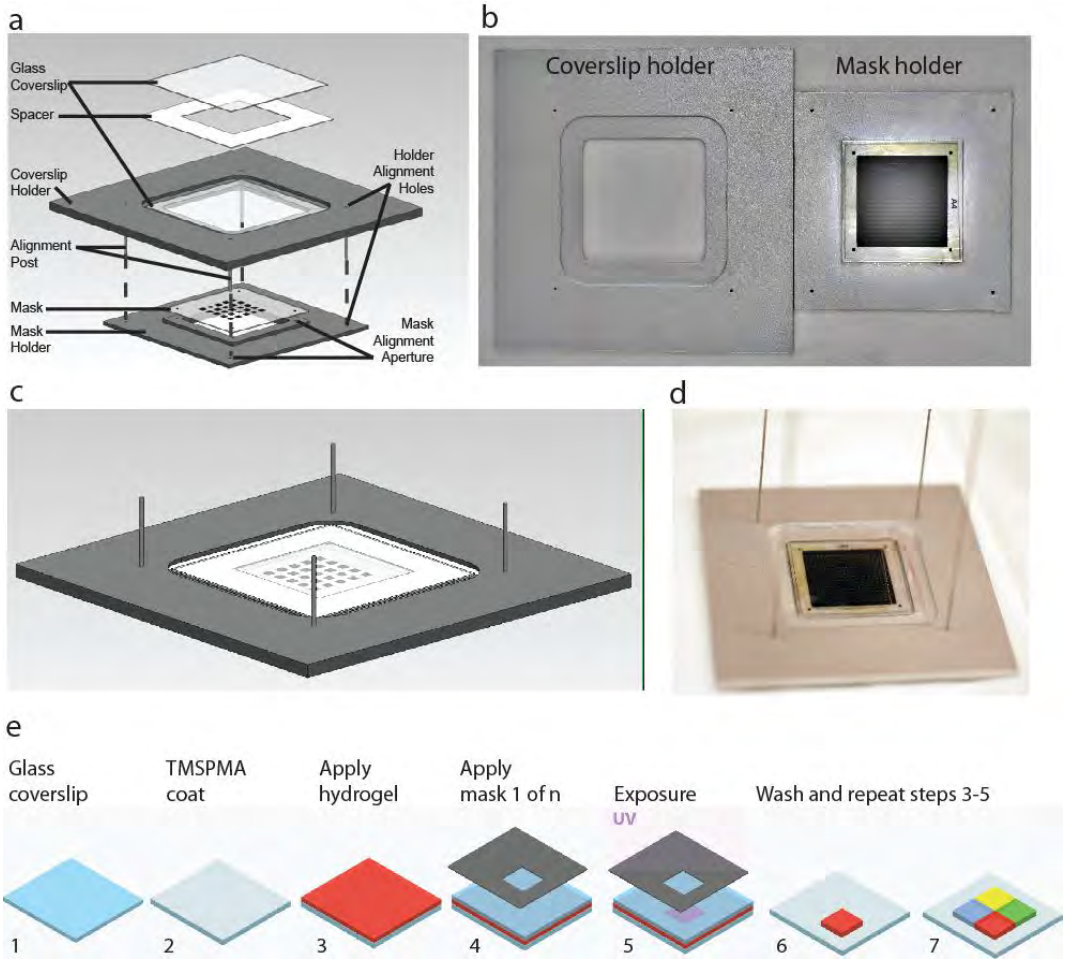

Figure s2: Mask alignment setup and protocol for digitally specified tissue prototypes

The mask alignment and digital sculpting device is composed of seven components (**Fig. s2**): fabrication compartment composed of a glass cover slip (i), spacer to control the thickness of each layer (ii), a treated glass cover slip on which the sculpted hydrogels are immobilized (iii),

fabrication chamber (iv) with alignment pins (v), the predesigned mask (vi) and a mask holder (vii) which aligns with the help of the pins on the chamber.

The precision of the alignment during fabrication was analyzed using NIH ImageJ program (developed at the U.S. National Institutes of Health and available at http://rsb.info.nih.gov/nih-image/). Region of interests (ROIs) were selected and analyzed using 4x microscope images (**Fig. s3a**) for square, radially fractioned circular (radial circular) and concentric circular geometries. The centroids of individual building blocks were determined using the centroid function in ImageJ. The centroid of the first unit was used as the reference point in determining the alignment precision of the remaining units based on the computer aided design coordinates (**Tables s2-s4**). The differences in X and Y axes and the total distance between the centroids of the building blocks were measured in reference to the first crosslinked unit's centroid (**Fig. s3b**). The alignment precision was reported in X, Y axes and in total distance between the centroids (**Fig. s3c**). The method achieved high alignment precision in digital sculpting tissue prototypes: 10.9 μm (±8.2 μm) for square geometry, 11.2 μm (±4.5 μm) for radial circular geometry, and 27.8 μm (±9.8 μm) for concentric circular geometry (mean ± STD, n = 16-24 measurements for each geometry). As the alignment precision was analyzed and presented in all directions for multiple samples, the same alignment precision would hold across layers as also displayed in Figure 4 for three different geometries since the same set of masks with the same alignment pins are used. We did not observe a change in alignment precision across layers within the 3 layers that were fabricated.

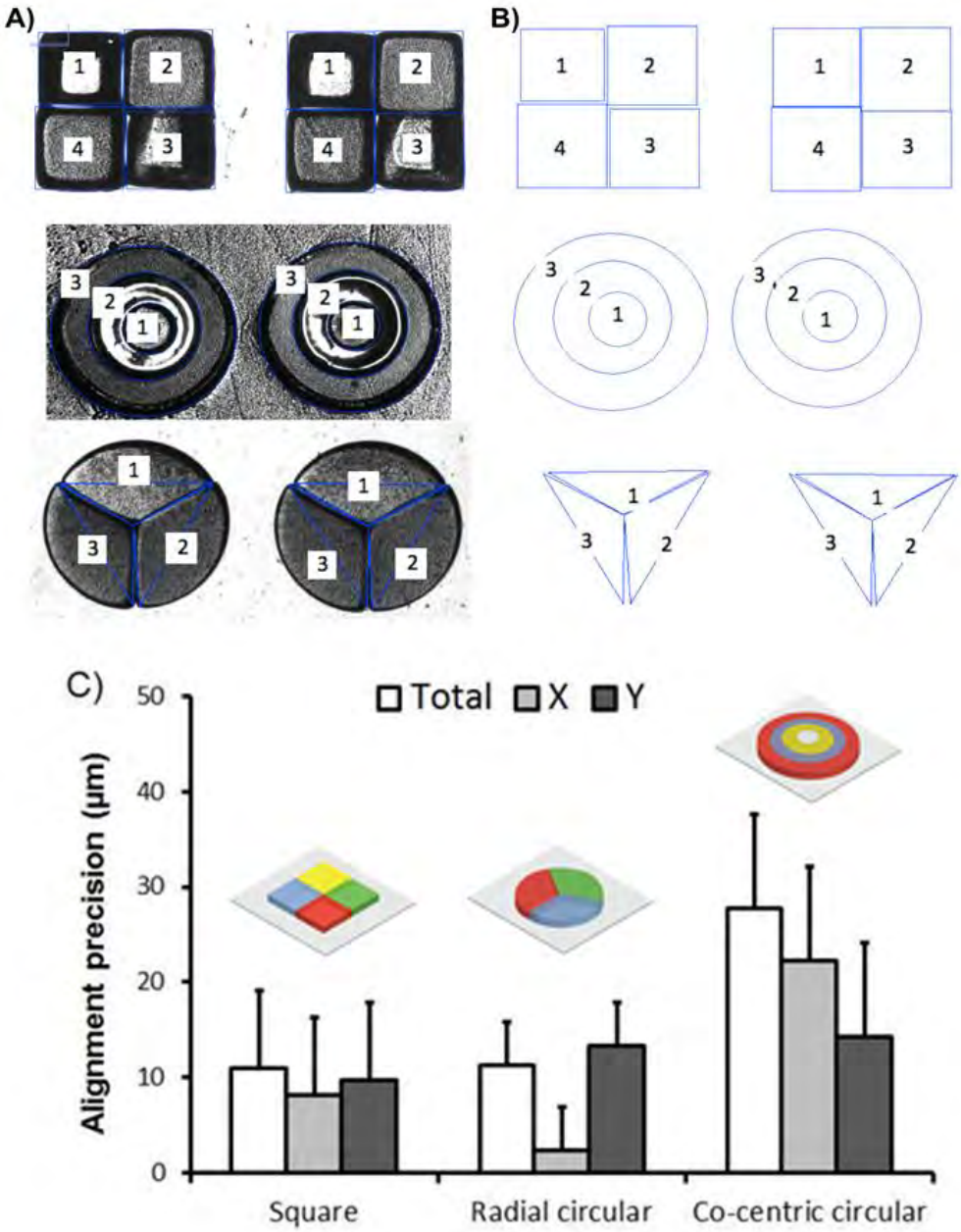

Figure s3: Quantification of alignment precision for square, radial circular, and concentric circular geometry tissue prototypes. a) Typical microscope images, and b) alignment markers used for quantification. c) Quantified alignment precision for tissue prototypes in X, Y directions and the total distance. The method achieved high alignment precision in digital sculpting tissue prototypes: 10.9 µm (±8.2 µm) for square geometry, 11.2 µm (±4.5 µm) for radial circular geometry, and 27.8 µm (±9.8 µm) for concentric circular geometry (mean ± standard deviation, n = 16-24 measurements each). Error bars in the figure represent mean ± standard deviation of the mean.

Gelatin (Type A, 300 bloom from porcine skin), methacrylic anhydride (MA) and 3-(trimethoxysilyl) propyl methacrylate (TMSPMA) were purchased from Sigma-Aldrich (St. Louis, MO). Photoinitiator 2-hydroxy-1-[4-(hydroxyethoxy)-phenyl]-2-methyl-lpropanone (Irgacure 2959) was purchased from Ciba Geigy (Igracure^{TM} 2959, Ciba Speciality

Chemicals, Tarrytown, NY, USA). The live/dead viability/cytotoxicity kit for mammalian cells was purchased from Invitrogen Corporation (Molecular Probes, Invitrogen, Carlsbad, USA). Neurobasal™, MEM and B27 supplement were purchased from Invitrogen Corp. (Carlsbad, CA). Glass slides and coverslips (VWR VistaVision™ microscope cover glasses, 25 × 25 mm) were purchased from Fisher Scientific (Philadelphia, USA).The Omnicure® S2000 UV/Visible Spot Curing System from EXPO Photonic Inc. (Ontario, CANADA) was used to polymerize hydrogels. We used the following antibodies: mouse monoclonal anti-Tau-1 (Millipore Bioscience Research Reagents, Darmstadt, GERMANY), rabbit polyclonal anti-GFAP (1:500 dilution; DakoCytomation), mouse anti-GAD65 (Millipore Bioscience Research Reagents, USA), rabbit anti-CaMKII (Santa Cruz Biotechnology, USA); Alexa Fluor® 488 goat anti-mouse IgG (Invitrogen, Carlsbad, CA, USA) and Alexa Fluor® 568 goat anti-rabbit IgG (Invitrogen, Carlsbad, CA, USA) were used as secondary antibody. The fabricated tissue prototypes were stained with Procion MX dyes (Sigma-Aldrich, St. Louis, MO, USA) in four different colors: red, blue, green, and yellow.

Gelatin methacrylate (GelMA) was dissolved at 10 % (w/v) gelatin (Type A, 300 bloom from porcine skin) in Dulbecco's phosphate buffered saline (DPBS; GIBCO) at 50 ºC for 1 hour. Methacrylic anhydride (94 %, MA, Sigma-Aldrich, St. Louis, MO) was added at 50 ºC under stirring condition for 2 hours. The solution was dialyzed in distilled water using a 12-14 kDa dialysis bag (Fisher Scientific, Philadelphia, USA) for 1 week at 40 ºC. The dialyzed solution was then transferred into 50 mL centrifuge tubes and lyophilized for one week to synthesize usable GelMA in powder form. GelMA precursor solution was prepared by mixing 5% (wt/wt) gelatin methacrylate and 1% (wt/wt) 2-hydroxy-1-(4-(hydroxyethoxy)phenyl)-2-methyl-1-propanone photo-initiating powder (Igracure™ 2959, Ciba Speciality Chemicals, Tarrytown, NY, USA) in DPBS with or withour cells.

In accordance with institutional guidelines for care and use of animals, dissociated cortical neurons were isolated. Briefly, neural cortex was extracted from postnatal 1 day old (PD 1) Sprague Dawley® rats (Charles River Labs, MA, USA). Cortex tissue was dissociated by trituration after digestion using papain (20 U/ml). The cells were then suspended in neurobasal medium with B27 supplement and 500 μM glutamine. The medium for new cultures was supplemented with 25 μM glutamate and 25 μM ß-mercaptoethanol. Cultured neurons were then suspended in GelMA precursor solution. Glass cover-slips with neuron-encapsulated tissue elements were placed in a six-well plate, and supplemented with 3 mL neural culture medium. Culture conditions were maintained at 37 ºC with a 95% relative humidity, and 5 % CO_2. Media was changed biweekly by replacing half with fresh media. To assess the viability of neurons in tissue constructs, live/dead assay (Molecular Probes, Invitrogen, Carlsbad, CA, USA) were conducted over time. Neuron encapsulating elements were incubated with live/dead staining solution that was composed of 4 μL ethidium homodimer-1 and 1 μL calcein-AM. Fluorescent images were taken (Nikon T2000) and NIH ImageJ software was used to analyze the images and quantify the results. Cell viability assay was conducted on days 0, 3 and 6. Long-term culture characterization included the neurite growth analysis **(Supplementary Video)** and functional immunostaining of the encapsulated neurons in 3D elements at the end of a 3-week culture period.

Functional immunofluorescent staining to identify cellular composition in digitally specified neural tissue constructs. The glass slides with neuron cell encapsulating elements were fixed with 4 % paraformaldehyde and permeabilized for 30 min with 0.5 % Triton X-100 and then blocked with 10 % goat serum albumin in phosphate buffered solution. These glass slides were washed with PBS and incubated separately with mouse monoclonal anti-Tau-1 / rabbit polyclonal anti-GFAP, mouse anti-GAD65 / rabbit anti-CaMKII, or mouse monoclonal anti-Tau-1 / rabbit anti-CaMKII, overnight at 4 ºC. After washing with PBS, glass slides were

incubated overnight at 4 ºC with Alexa Fluor® 488 goat anti-mouse IgG / Alexa Fluor® 568 goat anti-rabbit IgG secondary antibodies, as well as DAPI (Invitrogen, Carlsbad, CA, USA). The slides were transferred onto 24 × 60 mm glass slides and mounted using SlowFade® Gold antifade reagent (Invitrogen, Carlsbad, CA, USA) and scanned with a confocal microscope and imaged. The z-stacks were then merged using NIH ImageJ, and a video **(Supplementary Video)** showing 3D neural network cultured in elements was made with Imaris software (Bitplane Inc., South Windsor, CT).

Cell encapsulation and tracking in digitally specified tissue constructs. Three cell types were used: embryonic stem cells (ESCs), human umbilical vein endothelial cells (HUVECs), and NIH 3T3 fibroblasts. ESCs were cultured in Glasgow Minimum Essential Medium (Sigma Aldrich, USA) supplemented with 15% Fetal bovine serum (Invitrogen, Carlsbad, CA, USA) and 1% Penicillin Streptomycin (Invitrogen, Carlsbad, CA, USA) 1% Sodium Pyruvate (Invitrogen, Carlsbad, CA, USA) , 1% Non-essential amino acids (NEAA) (Invitrogen, Carlsbad, CA, USA), 0.1% B-mercaptoethanol (Invitrogen, Carlsbad, CA, USA) and 0.01% Leukemia Inhibitory Factor (MilliporeDarmstadt, Germany). HUVECs were cultured in Endothelial Cell Medium (Sigma). 3T3 cells were cultured in Dulbecco's Modified Eagle Medium (DMEM, Invitrogen) supplemented with 10% Fetal bovine Serum (FBS, Invitrogen) and 1% Penicillin Streptomycin (Invitrogen, Carlsbad, CA, USA). ESC, HUVEC and 3T3 cells were trypsinized and resuspended in hydrogel precursor solution (1:1 for cell medium suspension and GelMA solution) with a final concentration of $1x10^6$ cells/ml. For cell tracking test, cells were incubated with ER-Tracker™ 30 minutes before being resupended in hydrogel precursor solution: Red (BODIPY® TR glibenclamide, Invitrogen) for HUVEC, ER-Tracker™ Green (BODIPY® FL glibenclamide, Invitrogen) for ESCs, and ER-Tracker™ Blue-White DPX (Invitrogen, Carlsbad, CA, USA) for 3T3 cells. The multiple cell type encapsulating multi-element tissue prototypes were then fabricated following the protocol

described above. Florescent images of the tissue prototypes labeled with cell tracker were taken using an inverted microscope (Nikon TE2000).

Assessing cell viability in long-term culture of digitally specified tissue prototypes. Cell viability was tested using a live/dead assay at day 0, day 2, and day 3. Tissue prototypes for cell live/dead assay were prepared using cells without cell tracker stains. Tissue prototypes were first washed with DPBS and gels were incubated with 0.5 μl/ml of calcein-AM (for live cells) and 2 μl/ml of ethidium bromide (for dead cells) in DPBS. The fluorescent images were taken using an inverted microscope (Nikon TE2000). Cell viability was calculated as the average value of the fraction of live cells to the total number of cells taken from 5 samples. Viability of three different cell types encapsulated at varying concentrations, ESCs ($5x10^5$ cells/ml), HUVEC ($7.5x10^5$ cells/ml) and 3T3 ($1x10^6$ cells/ml), was quantified in fluorescent microscope images using the NIH ImageJ program (developed at the U.S. National Institutes of Health and available at http://rsb.info.nih.gov/nih-image/). We cultured the prototypes with a mixed medium (1:1:1 ratio of ESC: HUVEC: 3T3 media) for a period of up to 3 days. Cell culture medium was changed daily.

Coloring of hydrogels. A single batch of 40% PEG solution with a 1% photo initiator concentration (Igracure^{TM} 2959, Ciba Speciality Chemicals, Tarrytown, NY, USA) was prepared which was then divided into equal volumes and colored with Procion MX Dyes (Sigma-Aldrich, St. Louis, MO, USA). Two factors were taken into consideration when determining dye percentages: desired color intensity and the crosslinking quality of the colored gel. An optimization among the two gave lead to the following dye percentages in the hydrogel solution (**Table s1**).

Statistical analysis. The experimental results on the effects of UV intensity (n=3), photocrosslinking time (n=3-8), and culture duration (n=3-8) on cell viability; and the effect of element size and culture duration on axon length (n=3-6) were analyzed by performing

analysis of variance (ANOVA) with Tukey's posthoc test for multiple comparisons. The statistical comparisons between the neuron and glial cells (n=4), between the excitatory and inhibitory cells (n=5) were performed by non-parametric Mann-Whitney U test. Statistical significance threshold was set at 0.05 ($p<0.05$) for all analyses. Data are presented as mean ± standard deviation (STD) of the mean.

Table s1: Percentages of the dyes added to the PEG hydrogel solution and their relative cross-linking times

Color	%	Crosslink (sec)
Red	2.5	28
Blue	1.2	29
Green	1.9	29
Yellow	2.17	25
Orange	2.33	26.5

Table s2: Designed distances between centers of geometries according to a reference point of the first-crosslinked geometry's center

Number of Geometries (Fig S4 B)	Squares	Concentric Circular	Radial Circular
Difference between 1-2	500 μm	0 μm	288.7 μm
Difference between 1-3	707.1 μm	0 μm	288.7 μm
Difference between 1-4	500 μm	-	-

Table s3: Designed differences in X axis according to a reference point of the first-crosslinked geometry's center

Number of Geometries (Fig S4 B)	Squares	Concentric Circular	Radial Circular
Difference between 1-2	+500 μm	0 μm	+144.3 μm
Difference between 1-3	+500 μm	0 μm	-144.3 μm
Difference between 1-4	0 μm	-	-

Table s4: Designed differences in Y axis according to a reference point of the first-crosslinked geometry's center

Number of Geometries (Fig S4 B)	Squares	Concentric Circular	Radial Circular
Difference between 1-2	0 μm	0 μm	-250 μm
Difference between 1-3	-500 μm	0 μm	-250 μm
Difference between 1-4	-500 μm	-	-

Acknowledgements

We acknowledge Dr. Imran Rivzi for help with confocal imaging. Yantao Fan's salary was supported by Medical Systems Biology Research Center at the School of Medicine at Tsinghua University (Beijing 100084, PR China) for one year as a visiting researcher at BAMM Laboratories. Emel Sokullu Urkac's salary was supported by TUBITAK (The Scientific & Technological Research Council of Turkey, BIDEB 2219, Turkey) for one year as a visiting researcher at BAMM Laboratories. Dr. Feng Xu is currently at: Biomedical Engineering and Biomechanics Center and School of Life Science & Technology, Xi'an Jiaotong University, China.